JOURNAL OF GEOPHYSICAL RESEARCH, VOL. 101, NO. A4, PAGES 7923–7934, APRIL 1, 1996

Lorentzian ion exosphere model

V. Pierrard and J. Lemaire

Institut d'Aéronomie Spatiale de Belgique, Brussels, Belgium

Abstract. Since observed velocity distributions of particles in the magnetosphere generally have a suprathermal tail instead of an exponential one, we propose to recalculate the density and temperature distributions in a nonrotating ion exosphere with a Lorentzian velocity distribution function (VDF) instead of a Maxwellian. The number density, the flux of particles, parallel and perpendicular pressures, and energy flux of the different classes of particles in the exosphere have been determined for any value of the index κ characterizing the Lorentzian VDF. The barometric density and temperature distributions for a Maxwellian VDF and for a Lorentzian VDF are compared. It is shown that for particles in an attractive potential, the barometric density decreases more slowly with altitude for the Lorentzian VDF. Furthermore, the temperature increases with altitude in this case, while for a Maxwellian VDF, it is independent of altitude. It is suggested that positive gradients of the ion and electron temperatures observed between the topside ionosphere and the outer plasmasphere can be explained by this effect, that is, a non-Maxwellian VDF with an enhanced suprathermal tail.

Introduction

The velocity distribution function $f(\mathbf{r}, \mathbf{v}, t)$ of charged particles in an ion exosphere is a solution of the Boltzmann equation which, for steady state conditions, is equal to

$$(\mathbf{v_i}.\nabla_\mathbf{r})f_i + (\mathbf{a_i}.\nabla_\mathbf{v})f_i = \left(\frac{\delta f}{\delta t}\right)_c \qquad (1)$$

where $\mathbf{v_i}$ is the velocity of the particles and $\mathbf{a_i}$ is their acceleration in the gravitational potential (ϕ_g) and electrostatic potential (V): $\mathbf{a_i} = -\nabla(\phi_g + Z_i eV/m_i)$. The right-hand side (RHS) of (1) represents the rate of change of the velocity distribution function (VDF) due to collisions. At high altitude in the atmosphere and ionosphere, the collision frequency becomes so small that the RHS can be neglected in a first approximation. In the collisionless case, (1) is sometimes called the Vlasov equation.

As a consequence of Liouville's theorem, any function $f(c_1, c_2, ...)$, where $c_1, c_2, ...$ are the constants of the motion of the particles in the gravitational field, electric field and magnetic field is a solution of the collisionless Boltzmann or Vlasov equation. In the absence of collisions, the total energy of the particles is conserved: $c_1 = (m_i v^2)/2 + m_i\phi_g + Z_i eV$. In the presence of a magnetic field, the magnetic moment of the particles is an adiabatic invariant, provided the Alfvèn conditions are satisfied: $c_2 = (m_i v_\perp^2)/2B$.

Paper number 95JA03802.
0148-0227/96/95JA-03802$05.00

The Maxwellian VDF is defined by

$$f_i^M(\mathbf{r}, \mathbf{v}) = \frac{n_{0i}}{(\pi w_i^2)^{3/2}} \exp\left(\frac{-v^2}{w_i^2}\right) \cdot \exp\left\{ - \frac{m_i\phi_g(\mathbf{r}) + Z_i eV(\mathbf{r})}{kT_{0i}} \frac{-m_i\phi_g(\mathbf{r}_0) - Z_i eV(\mathbf{r}_0)}{kT_{0i}} \right\} \qquad (2)$$

where m_i is the mass of the particles, n_{0i} is the number density, T_{0i} the temperature of the particles at a reference level r_0, and $w_i = \sqrt{2kT_{0i}/m_i}$ the thermal speed. The ϕ_g symbol represents the gravitational potential, and V is the electrostatic potential which is induced by the slight charge separation of electrons and ions in the gravitational field. The resulting polarization electric field maintains the plasma quasi-neutral. It is convenient to introduce $q_i(\mathbf{r})$, the dimensionless potential energy of a particle by

$$q_i(\mathbf{r}) = \frac{R(\mathbf{r})}{w_i^2} = \frac{m_i\phi_g(\mathbf{r}) + Z_i eV(\mathbf{r}) - m_i\phi_g(\mathbf{r}_0) - Z_i eV(\mathbf{r}_0)}{kT_{0i}}. \qquad (3)$$

At r_0, $q_i = 0$. When the total potential energy of a particle is increasing with altitude, $q_i(\mathbf{r})$ is a positive and increasing function of r for $r > r_0$. In this case, the total force is attractive, that is, directed toward the planet. On the contrary, when the total potential is a repulsive one, $q_i(\mathbf{r})$ is a negative and decreasing function of r for $r > r_0$.

Since $f_i^M(\mathbf{r},\mathbf{v})$ is a function of the total energy $E_i = (m_i v^2)/2 + q_i(\mathbf{r})kT_{0i}$ which is a constant of the motion, this VDF is necessarily a solution of the collisionless Boltzmann equation. Note that in the case of a collision dominated gas, $f_i^M(\mathbf{r},\mathbf{v})$ is also a solution of (1) when the system is at equilibrium.

Although generally adopted in exospheric models like those of *Lemaire and Scherer* [1970, 1973, 1974, 1983], *Knight* [1973], *Chiu and Schulz* [1978], *Chiu et al.* [1981], *Fridman and Lemaire* [1980], *Lyons* [1980, 1981], and *Stern* [1981], the Maxwellian VDF is not the only solution of the Vlasov equation: there are an infinite number of collisionless solutions. The Lorentzian function $f_i^\kappa(\mathbf{r},\mathbf{v})$ is one of them. Indeed, it depends only on the total energy of the particles which is a constant of motion.

The Lorentzian or kappa function is defined by

$$f_i^\kappa(\mathbf{r},\mathbf{v}) = \frac{n_{0i}}{2\pi(\kappa w_i^2)^{3/2}} \frac{\Gamma(\kappa+1)}{\Gamma(\kappa-1/2)\Gamma(3/2)} \cdot \left(1+\frac{v^2+R(\mathbf{r})}{\kappa w_i^2}\right)^{-(\kappa+1)} . \quad (4)$$

where $\Gamma(x)$ is the gamma function and $R(r)$ is given by (3).

For velocities v smaller or comparable to w_i, the Lorentzian VDF is rather close to the Maxwellian having the same thermal speed for any value of $\kappa > 2$. The value of the index κ determines the slope of the energy spectrum of the suprathermal particles forming the tail of the VDF. For $v >> w_i$, the Lorentzian VDF decreases with v as a power law ($f \sim v^{-2(\kappa+1)}$) [*Christon et al.*, 1988]. The smaller the value of κ, the harder is the energy spectrum. It can be verified that the integral of f_i^κ over the whole velocity space is equal to the particle density n_{0i}. Furthermore, w_i is determined by the second-order moment of $f_i^\kappa(\mathbf{r},\mathbf{v})$, that is, $p_i = m_i \int f_i^\kappa(\mathbf{r},\mathbf{v}) v^2 \, d^3v = n_{0i}kT_{0i}\kappa/(\kappa - 3/2) = m_i w_i^2 \kappa/(2\kappa - 3)$.

In the limit $\kappa \to \infty$, the kappa function degenerates into a Maxwellian f^M with the density n_{0i} and temperature T_{0i}. Therefore the kappa functions form a wider class of VDF than the Maxwellian which is generally used in theoretical models or to fit observed velocity distributions. The VDFs of space plasmas, and in particular of the Earth's magnetosphere, usually have non-Maxwellian suprathermal tails [*Gloeckler and Hamilton*, 1987; *Lui and Krimigis*, 1981, 1983; *Williams et al.*, 1988] where $f(\mathbf{r},\mathbf{v})$ decreases as a power law of the velocity [*Bame et al.*, 1967]. The origin of these non-Maxwellian distributions is not yet clear. Nevertheless, Lorentzian distributions are very useful fit functions both for small particle velocities as well as for suprathermal ones.

Figure 1 illustrates the distributions of field aligned velocities $f(r, v_\parallel)$ as a function of $v_\parallel/w$ in the case of a Maxwellian VDF (curve 1) and of a kappa VDF corresponding to $\kappa = 5$ (curve 2). The density n_0 and the temperature T_0 are the same for both VDFs. The curves 1 and 2 refer to the VDF at the reference level r_0, where $q_i(r_0) = 0$. The curves 3 and 4 correspond respectively to the Maxwellian VDF and kappa VDF for $\kappa = 5$ but at a higher altitude $r > r_0$ where $q(\mathbf{r}) > 0$, that is, when the total potential increases with altitude. On Figure 1b, all VDFs are normalized to unity at $v_\parallel = 0$. Note that the normalized curves 1 and 3 corresponding to the Maxwellian VDF respectively at r_0 and $r > r_0$ are identical; this implies that the dispersion of velocities is the same at all altitudes in the exosphere where the VDF is Maxwellian. The temperature $T(\mathbf{r})$ is then independent of the altitude and equal to T_0. The exosphere is isothermal if the VDF is a Maxwellian at the reference level. The reason for this property is that for the Maxwellian VDF given by (2), the velocity variables (v_x, v_y, v_z) and spatial coordinates (x, y, z) are separable. However, this is not the case for the kappa VDF given by (4) : the dispersion of the velocities depends then on the value of $q_i(\mathbf{r})$ which is a function of the spatial variable r.

It will be shown below that the temperature $T_i(\mathbf{r})$ characterizing a kappa VDF is an increasing function of altitude when $q_i(\mathbf{r})$ is also an increasing function of r. This is illustrated on Figure 1 where the wings of the curve 4 have a smaller slope (at $r > r_0$) than those of curve 2 (at $r = r_0$). Note that the positive temperature gradient is a consequence of the suprathermal tails of the distributions. Any distribution which simulates a suprathermal particle population would also lead to a temperature increasing with altitude.

This effect has been called the "velocity filtration effect" by *Scudder* [1992a, b] who applied it to explain the high temperature observed in the solar corona. Assuming that the VDF in the chromosphere is non-Maxwellian for example, a kappa function with $\kappa = 2.5 - 7$, he found that the dispersion of the VDF and plasma temperature increases from 10,000 K at the altitude of the chromosphere up to $1-2\times10^6$ K in the solar corona without the need of any ad hoc or extra heat deposition at high altitude. The high coronal temperature is then, according to Scudder, a straightforward consequence of the velocity filtration effect.

The purpose of this paper is to point out that the velocity filtration effect can be applied to the topside ionosphere and can equally well explain the increase of the plasma temperature as a function of altitude in the outer plasmasphere and plasmathrough. Assuming that the tail of the VDF formed by the suprathermal particles in the topside ionosphere is approximately a power law with an index $\kappa = 3 - 4$, we will show in the following paragraphs that the temperature characterizing the spread of the VDF increases in the outer plasmasphere region up to values of $10 - 20 \times 10^3$ K which are comparable to those measured with satellites at high altitudes [*Gringauz and Bezrukikh*, 1976; *Norris et al.*,

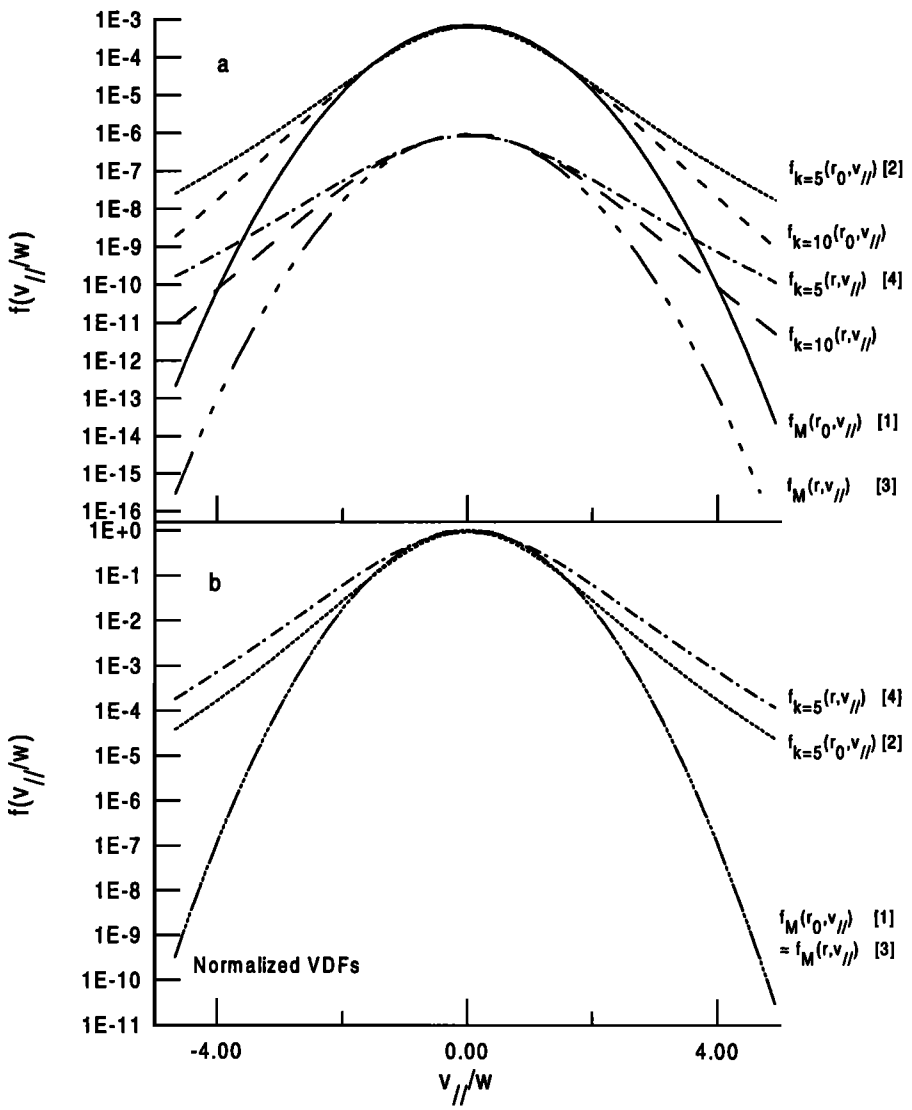

Figure 1. (a) Curves 1 and 2 represent respectively a Maxwellian VDF and a Lorentzian VDF ($\kappa = 5$) with the same temperature and density at $r_0 = 3000$ km. Curves 3 and 4 represent respectively the Maxwellian VDF and the Lorentzian VDF ($\kappa = 5$) for $r > r_0$, in an attractive potential. Comparison is also shown with a Lorentzian VDF for $\kappa = 10$. (b) Normalized velocity distributions (curves 1 to 4). In the case of the Maxwellian VDF (curves 1 and 3), the temperature is independent of altitude and equal to T_0. For the kappa VDF (curves 2 and 4), the dispersion of velocities increases when r increases; the temperature characterizing the spread of velocity increases with altitude. This is not the case for a Maxwellian VDF. Indeed, when the VDF is Maxwellian at the exobase, the exosphere is isothermal: $T(\mathbf{r}) = T_0$.

1983; *Gringauz*, 1985; *Comfort et al.*, 1985; *Farrugia et al.*, 1989].

In order to calculate the temperature distribution in an ion exosphere when the VDF is a kappa function, analytic expressions for the moments of this VDF must be determined. The derivation of the mathematical expressions for the particle density $n(\mathbf{r}) = \int f(\mathbf{r},\mathbf{v})\, d^3v$, the particle flux parallel to the field lines $F(\mathbf{r}) = \int v_{\|} f(\mathbf{r},\mathbf{v})\, d^3v$, the parallel and perpendicular momentum flux $P_{\|}(\mathbf{r}) = m \int v_{\|}^2 f(\mathbf{r},\mathbf{v})\, d^3v$ and $P_{\perp}(\mathbf{r}) = \frac{1}{2} m \int v_{\perp}^2 f(\mathbf{r},\mathbf{v})\, d^3v$, the energy flux parallel to the magnetic field $E(\mathbf{r}) = \frac{1}{2} m \int v^2 v_{\|} f(\mathbf{r},\mathbf{v})\, d^3v$ is given in the next section. Those who are interested in the physical results and application of these formulae to the ionosphere-plasmasphere system more than in their derivation may skip to section 3.

Moments of a Lorentzian Velocity Distribution Function

The kinetic model of the ion exosphere developed by *Lemaire and Scherer* [1970, 1971] for geomagnetic field

lines open to the magnetospheric tail rest on the assumption that the ion and electron VDFs are Maxwellian. Since in the magnetospheric plasma, the velocity distribution functions have generally a non-Maxwellian suprathermal tail, we propose to develop in this section a model of ion exosphere similar to the models of *Lemaire and Scherer* [1970, 1971], but with a kappa distribution function instead of a Maxwellian one. We determine the analytic expressions for the moments of the kappa VDF and compare them with those of the Maxwellian model.

We consider a collision-dominated barosphere, separated from the exosphere by a transition region where the Coulomb collisions cannot be neglected but are not sufficient to keep a Maxwellian distribution. The parameter κ is expected to be determined by the energy-dependent collision rate in the transition region. The upper frontier of this transition region is called exobase or baropause. Above this surface (i.e. in the exosphere), the collisions are assumed to be unimportant. *Spitzer* [1949] argued that this transition altitude can be chosen as the height at which the mean free path of the particles equals the density scale height. For charged particles, this exobase level where $r = r_0$ is rather high, and we will assume its altitude to be 3000 km.

The particles are moving along dipolar magnetic field lines. Their trajectories can be divided in four different classes depending on their velocity and pitch angle. According to the terminology of *Lemaire and Scherer* [1974], there are trapped, incoming, escaping, and ballistic particles (cf. Tables 1 and 2). The ballistic particles emerge from the barosphere but do not have enough kinetic energy or are reflected magnetically before reaching the equator. These particles spiral up in the exosphere and fall back in the same hemisphere. The escaping particles leave one hemisphere and reenter in the barosphere in the other hemisphere. The incoming particles are particles coming from the other hemisphere. Finally, the trapped particles bounce up and down between two mirror points in the ion exosphere. Each of these classes of particles will contribute to the exospheric density, flux of particles, pressure tensors and energy flux [*Fälthammar*, 1983]. These contributions will be determined separately.

We use the spherical polar coordinates (v, θ, ϕ) with the polar axis tangent to the magnetic field. In each class of particle orbits, ϕ varies from 0 to 2π. The velocities v and pitch angles θ whose determine each class of particles are summarized in Tables 1 and 2.

Table 1. Classes of Particles According to Their Velocity $v(\mathbf{r})$ and Pitch Angle $\theta(\mathbf{r})$ at the Radial Distance r in Case a When the Velocity of an Upward Moving Particle Decreases Monotonically With Altitude, i.e. When $q(\mathbf{r})$ Is Increasing With r

$v(\mathbf{r})$	$\theta(\mathbf{r})$	Class
$[v_\infty, \infty]$	$[0, \theta_m(\mathbf{r})]$	Escaping
$[v_b(\mathbf{r}), v_\infty(\mathbf{r})]$	$[0, \theta_m(\mathbf{r})], [\pi - \theta_m(\mathbf{r}), \pi]$	Ballistic
$[0, v_b(\mathbf{r})]$	$[0, \pi]$	Ballistic
$[v_\infty, \infty]$	$[\theta_m(\mathbf{r}), \pi]$	Incoming
$[v_b(\mathbf{r}), v_\infty(\mathbf{r})]$	$[\theta_m(\mathbf{r}), \pi - \theta_m(\mathbf{r})]$	Trapped

Table 2. Classes of Particles According to Their Velocity $v(\mathbf{r})$ and Pitch Angle $\theta(\mathbf{r})$ at the Radial Distance r in Case b When the Velocity of an Upward Moving Particle Increases Monotonically With Altitude, i.e. When $q(\mathbf{r})$ Is Decreasing With r

$v(\mathbf{r})$	$\theta(\mathbf{r})$	Class
$[v_\psi(\mathbf{r}), \infty]$	$[0, \theta_m(\mathbf{r})]$	Escaping
$[v_\psi(\mathbf{r}), \infty]$	$[\theta_m(\mathbf{r}), \pi]$	Incoming
$[0, v_\psi(\mathbf{r})]$	$[0, \pi]$	Incoming

We assume that the trapped and incoming particles which reach the baropause have the same velocity distribution as the barospheric particles but multiplied respectively by weight factors ξ and ζ. If these factors are equal to 1, the exospheric particles are in thermal equilibrium with those emerging from the barosphere. The pitch angle distribution is then isotropic. Putting respectively $\xi = 0$ or $\zeta = 0$ means that the trapped or incoming particles are missing in the VDF.

The density, flux, pressure, and energy flux correspond respectively to the moments of zero, first, second, and third order of the Kappa VDF. When the potential energy of the particles $q_i(\mathbf{r})$ is an increasing function of $\mathbf{r}$, the moments of the VDF up to the third order are given by

Ballistic Particles

$$n(\mathbf{r}) = n_0 \left(1 + \frac{R}{\kappa w^2}\right)^{-(\kappa+1)} \cdot[d^{3/2}(1 - \beta_2(b)) - \alpha c^{3/2}(1 - \beta_2(f))] \quad (5)$$

$$F(\mathbf{r}) = 0 \quad (6)$$

$$P_{\|}(\mathbf{r}) = \frac{1}{3} n_0 m w^2 \frac{A_k}{A_k'} \kappa \left(1 + \frac{R}{\kappa w^2}\right)^{-(\kappa+1)} \cdot[d^{5/2}(1 - \beta_4(b)) - \alpha c^{5/2} p(1 - \beta_4(f))] \quad (7)$$

$$P_{\perp}(\mathbf{r}) = \frac{1}{3} n_0 m w^2 \frac{A_k}{A_k'} \kappa \left(1 + \frac{R}{\kappa w^2}\right)^{-(\kappa+1)} \cdot[d^{5/2}(1 - \beta_4(b)) - \alpha c^{5/2}(1 + \frac{\eta}{2})(1 - \beta_4(f)) - \frac{3}{2} \frac{\eta R}{p \kappa w^2} \alpha c^{3/2}(1 - \beta_2(f)) \frac{A_k'}{A_k}] \quad (8)$$

$$E(\mathbf{r}) = 0 \quad (9)$$

with

$$\frac{R(\mathbf{r})}{w^2} = q(\mathbf{r}) > 0 \quad (10)$$

$$= \frac{-m\Phi_g(\mathbf{r}_0) - ZeV(\mathbf{r}_0) + m\Phi_g(\mathbf{r}) + ZeV(\mathbf{r})}{kT_0}$$

$$\alpha = p^{1/2} \left(1 + \frac{\eta R}{p(\kappa w^2 + R)}\right)^{-(\kappa+1)} \quad (11)$$

$$c = 1 + \frac{R}{p \kappa w^2} \quad (12)$$

$$b = \left(1+\frac{V_\infty^2}{\kappa+R/w^2}\right)^{-1} \quad (13)$$

$$d = \left(1+\frac{R}{\kappa w^2}\right) \quad (14)$$

$$f = \left(1+\frac{X^2}{p\kappa+R/w^2}\right)^{-1} \quad (15)$$

$$V_\infty^2(\mathbf{r}) = \left(-\frac{m\Phi_g(\mathbf{r})}{kT_0}-\frac{ZeV(\mathbf{r})}{kT_0}\right)>0 \quad (16)$$

$$X^2 = pV_\infty^2-\eta R/w^2 \quad (17)$$

$$U_0 = \left(-\frac{m\Phi_g(\mathbf{r}_0)}{kT_0}-\frac{ZeV(\mathbf{r}_0)}{kT_0}\right)>0 \quad (18)$$

$$\eta = \frac{r_0^3}{r^3} \quad (19)$$

$$p = 1-\eta \quad (20)$$

$$A_k = \frac{\Gamma(\kappa+1)}{\Gamma(\kappa-1/2)\Gamma(3/2)} \quad (21)$$

$$A_k' = \frac{\Gamma(\kappa+1)}{\Gamma(\kappa-3/2)\Gamma(5/2)} \quad (22)$$

$$\beta_2(x) = \int_0^x A_k t^{\kappa-3/2}(1-t)^{1/2}dt \quad (23)$$

$$= 1-\int_x^1 A_k t^{\kappa-3/2}(1-t)^{1/2}dt$$

$$\beta_4(x) = \int_0^x A_k' t^{\kappa-5/2}(1-t)^{3/2}dt \quad (24)$$

$$= 1-\int_x^1 A_k' t^{\kappa-5/2}(1-t)^{3/2}dt$$

Escaping Particles

$$n(\mathbf{r}) = \frac{1}{2}n_0\left(1+\frac{R}{\kappa w^2}\right)^{-(\kappa+1)} \cdot[d^{3/2}\beta_2(b)-\alpha c^{3/2}\beta_2(f)] \quad (25)$$

$$F(\mathbf{r}) = \frac{\eta}{4}n_0\frac{w}{\kappa^{1/2}}\frac{A_k}{\kappa-1}(1+U_0)\left(1+\frac{U_0}{\kappa}\right)^{-\kappa} \quad (26)$$

$$P_\parallel(\mathbf{r}) = \frac{1}{6}n_0 m w^2\frac{A_k}{A_k'}\kappa\left(1+\frac{R}{\kappa w^2}\right)^{-(\kappa+1)} \cdot[d^{5/2}\beta_4(b)-\alpha c^{5/2}p\beta_4(f)] \quad (27)$$

$$P_\perp(\mathbf{r}) = \frac{1}{6}n_0 m w^2\frac{A_k}{A_k'}\kappa\left(1+\frac{R}{\kappa w^2}\right)^{-(\kappa+1)} \cdot[d^{5/2}\beta_4(b)-\alpha c^{5/2}(1+\frac{\eta}{2})\beta_4(f) -\frac{3}{2}\frac{\eta R}{p\kappa w^2}\alpha c^{3/2}\beta_2(f)\frac{A_k'}{A_k}] \quad (28)$$

$$E(\mathbf{r}) = \frac{\eta m}{8}n_0 A_k\kappa^{1/2}w\left(1+\frac{U_0}{\kappa}\right)^{-\kappa} \cdot\left\{(\kappa w^2)\left[\frac{1}{\kappa-2}\left(1+\frac{U_0}{\kappa}\right)^2 -\frac{2}{\kappa-1}\left(1+\frac{U_0}{\kappa}\right)+\frac{1}{\kappa}\right] +\frac{R}{w^2}\left[\frac{1+U_0}{\kappa(\kappa-1)}\right]\right\} \quad (29)$$

Trapped Particles

$$n(\mathbf{r}) = \xi n_0\left(1+\frac{R}{\kappa w^2}\right)^{-(\kappa+1)} \cdot[\alpha c^{3/2}(1-\beta_2(f))] \quad (30)$$

$$F(\mathbf{r}) = 0 \quad (31)$$

$$P_\parallel(\mathbf{r}) = \frac{\xi}{3}n_0 m w^2\frac{A_k}{A_k'}\kappa\left(1+\frac{R}{\kappa w^2}\right)^{-(\kappa+1)} \cdot[\alpha c^{5/2}p(1-\beta_4(f))] \quad (32)$$

$$P_\perp(\mathbf{r}) = \frac{\xi}{3}n_0 m w^2\frac{A_k}{A_k'}\kappa\left(1+\frac{R}{\kappa w^2}\right)^{-(\kappa+1)} \cdot[\alpha c^{5/2}(1+\frac{\eta}{2})(1-\beta_4(f)) +\frac{3}{2}\frac{\eta R}{p\kappa w^2}\alpha c^{3/2}(1-\beta_2(f))\frac{A_k'}{A_k}] \quad (33)$$

$$E(\mathbf{r}) = 0 \quad (34)$$

Incoming Particles

$$n(\mathbf{r}) = \zeta\frac{1}{2}n_0\left(1+\frac{R}{\kappa w^2}\right)^{-(\kappa+1)} \cdot[d^{3/2}\beta_2(b)+\alpha c^{3/2}\beta_2(f)] \quad (35)$$

$$F(\mathbf{r}) = -\zeta\frac{\eta}{4}n_0\frac{w}{\kappa^{1/2}}\frac{A_k}{\kappa-1}(1+U_0)\left(1+\frac{U_0}{\kappa}\right)^{-\kappa} \quad (36)$$

$$P_\parallel(\mathbf{r}) = \frac{1}{6}n_0 m w^2\frac{A_k}{A_k'}\kappa\left(1+\frac{R}{\kappa w^2}\right)^{-(\kappa+1)} \cdot[d^{5/2}\beta_4(b)+\alpha c^{5/2}p\beta_4(f)] \quad (37)$$

$$P_\perp(\mathbf{r}) = \zeta\frac{1}{6}n_0 m w^2\frac{A_k}{A_k'}\kappa\left(1+\frac{R}{\kappa w^2}\right)^{-(\kappa+1)} \cdot[d^{5/2}\beta_4(b)+\alpha c^{5/2}(1+\frac{\eta}{2})\beta_4(f) +\frac{3}{2}\frac{\eta R}{p\kappa w^2}\alpha c^{3/2}\beta_2(f)\frac{A_k'}{A_k}] \quad (38)$$

$$E(\mathbf{r}) = -\zeta\frac{\eta m}{8}n_0 A_k\kappa^{1/2}w\left(1+\frac{U_0}{\kappa}\right)^{-\kappa} \cdot\left\{\kappa w^2\left[\frac{1}{\kappa-2}\left(1+\frac{U_0}{\kappa}\right)^2 -\frac{2}{\kappa-1}\left(1+\frac{U_0}{\kappa}\right)+\frac{1}{\kappa}\right] +\frac{R}{w^2}\left[\frac{1+U_0}{\kappa(\kappa-1)}\right]\right\} \quad (39)$$

Similar expressions are obtained when the potential energy of the particles $q_i(\mathbf{r})$ is a decreasing function of r i.e. in a repulsive potential.

Escaping Particles

$$n(\mathbf{r}) = \frac{1}{2}n_0\left(1+\frac{R}{\kappa w^2}\right)^{-(\kappa+1)} \cdot[d^{3/2}\beta_2(b') - \alpha c^{3/2}\beta_2(f')] \quad (40)$$

$$F(\mathbf{r}) = \frac{\eta}{4}n_0\frac{w}{\kappa^{1/2}}\frac{A_k}{\kappa-1} \quad (41)$$

$$P_{\parallel}(\mathbf{r}) = \frac{1}{6}n_0 m w^2\frac{A_k}{A'_k}\kappa\left(1+\frac{R}{\kappa w^2}\right)^{-(\kappa+1)} \cdot[d^{5/2}\beta_4(b') - \alpha c^{5/2}p\beta_4(f')] \quad (42)$$

$$P_{\perp}(\mathbf{r}) = \frac{1}{6}n_0 m w^2\frac{A_k}{A'_k}\kappa\left(1+\frac{R}{\kappa w^2}\right)^{-(\kappa+1)} \cdot[d^{5/2}\beta_4(b') - \alpha c^{5/2}(1+\frac{\eta}{2})\beta_4(f') - \frac{3}{2}\frac{\eta R}{p\kappa w^2}\alpha c^{3/2}\beta_2(f')\frac{A'_k}{A_k}] \quad (43)$$

$$E(\mathbf{r}) = \frac{\eta m}{8}n_0 A_k \kappa^{1/2} w\left(\left(\frac{1}{\kappa}-\frac{2}{\kappa-1}+\frac{1}{\kappa-2}\right)\cdot(\kappa w^2)+\frac{R}{w^2\kappa(\kappa-1)}\right) \quad (44)$$

Incoming Particles

$$n(\mathbf{r}) = \zeta\frac{1}{2}n_0\left(1+\frac{R}{\kappa w^2}\right)^{-(\kappa+1)} \cdot[d^{3/2}(2-\beta_2(b') + \alpha c^{3/2}\beta_2(f')] \quad (45)$$

$$F(\mathbf{r}) = -\zeta\frac{\eta}{4}n_0\frac{w}{\kappa^{1/2}}\frac{A_k}{\kappa-1} \quad (46)$$

$$P_{\parallel}(\mathbf{r}) = \frac{\zeta}{6}n_0 m w^2\frac{A_k}{A'_k}\kappa\left(1+\frac{R}{\kappa w^2}\right)^{-(\kappa+1)} \cdot[d^{5/2}(2-\beta_4(b')) + \alpha c^{5/2}p\beta_4(f')] \quad (47)$$

$$P_{\perp}(\mathbf{r}) = \frac{\zeta}{6}n_0 m w^2\frac{A_k}{A'_k}\kappa\left(1+\frac{R}{\kappa w^2}\right)^{-(\kappa+1)} \cdot[d^{5/2}(2-\beta_4(b')) + \alpha c^{5/2}(1+\frac{\eta}{2})\beta_4(f') + \frac{3}{2}\frac{\eta R}{p\kappa w^2}\alpha c^{3/2}\beta_2(f')\frac{A'_k}{A_k}] \quad (48)$$

$$E(\mathbf{r}) = -\zeta\frac{\eta m}{8}n_0 A_k \kappa^{1/2} w\left(\left(\frac{1}{\kappa}-\frac{2}{\kappa-1}+\frac{1}{\kappa-2}\right)\cdot\kappa w^2+\frac{R}{\kappa w^2(\kappa-1)}\right) \quad (49)$$

with

$$\frac{R}{w^2} = \left(\frac{-mv_\psi^2}{2kT_0}\right) < 0 \quad (50)$$

$$= \frac{-m\Phi_g(\mathbf{r}_0) - ZeV(\mathbf{r}_0) + m\Phi_g(\mathbf{r}) + ZeV(\mathbf{r})}{kT_0}$$

$$b' = \left(1-\frac{R}{w^2(\kappa+R/w^2)}\right)^{-1} \quad (51)$$

$$f' = \left(1-\frac{R}{w^2(p\kappa+R/w^2)}\right)^{-1} \quad (52)$$

It can be verified that when $\kappa \to \infty$, these expressions tend to expressions of the Maxwellian model developed by *Lemaire and Scherer* [1970]. Indeed,

$$\lim_{\kappa\to\infty}(1+q(\mathbf{r})/\kappa)^{-\kappa} = \exp(-q(\mathbf{r})), \quad (53)$$

$$\lim_{\kappa\to\infty}\beta_2(b) = 2\left(\frac{1}{2}-K_2(V_\infty)\right) \quad (54)$$

where $K_2(x) = \int_0^x \frac{2}{\pi^{1/2}}t^2\exp(-t^2)dt$.

Density Distribution

The expressions (5) to (49) are quite general. They give the moments for a wide range of truncated Lorentzian VDF when ξ and ζ are arbitrary constant. The barometric case is always recovered when $\xi = \zeta = 1$. In this case, the expressions of the moments have much simpler forms since many terms in (5) to (49) cancel out.

Let us first examine the simplest ion exosphere (protonosphere) in barometric equilibrium for which the electrons and H^+ ions have the same density and the same temperatre at the reference level of 3000 km.

The mean free path of a test ion with a velocity equal to the average thermal ion velocity in a plasma consisting of electrons and one ion species can be evaluated by the formula of *Hinton* [1983]:

$$\lambda = \frac{3\sqrt{3}(4\pi\epsilon_0)^2(kT)^2}{4(2\pi)^{1/2}nZ^4e^4\ln\Lambda}. \quad (55)$$

where T is the temperature of the field particles, n is their density, $\epsilon_0 = 8.854 \times 10^{-12}$ C^2/(Nm^2) is the dielectric constant of vacuum, $k = 1.38 \times 10^{-23}$ J/K is the Boltzmann constant, $Z_i e$ is electric charge and $\ln\Lambda$ is the Coulomb logarithm.

The scale height can be estimated by

$$H = \frac{kT}{mg} \quad (56)$$

where m is the mean molecular mass ($=m_{H^+}/2$ in a protonosphere) and g is the gravitational acceleration.

It can be verified that for $T = 4000$ K and $n(\mathbf{r}_0) = 300$ cm^{-3}, $\lambda_i \sim H \sim 6631$ km. These density and temperature conditions were chosen so that the mean free path is equal to the density scale height at the exobase.

This condition implies that the collision rate is small in the ion exosphere above the exobase [*Spitzer*, 1956]. For larger plasma densities or smaller plasma temperatures, the plasma would be collision dominated. However, this does not imply that its velocity distribution should be necessarily purely Maxwellian in the transition region where the Knudsen number is of the order of 1.

When the VDF is Maxwellian and the pitch angle distribution is isotropic (i.e. $\xi = \zeta = 1$), the total density distribution is given by

$$n(\mathbf{r}) = n(\mathbf{r}_0) \exp(-R(\mathbf{r})/w^2), \tag{57}$$

which corresponds to the barometric model.

Similarly, when the VDF corresponds to the Lorentzian or kappa model and when the pitch angle distribution is isotropic, the total density distribution is obtained by summing the RHS of (5), (25), (30), and (35):

$$n(\mathbf{r}) = n(\mathbf{r}_0) \left(1 + \frac{R(\mathbf{r})}{\kappa w^2}\right)^{-\kappa+1/2}. \tag{58}$$

Note that these formula are applicable to neutral exosphere in which case the total potential $q_i k T_{0i}$ is determined only by the gravitational potential. In an ion exosphere, the distributions of electrons and ions are also dependent of the electrostatic potential. Note also that this density distribution corresponds to the state of hydrostatic equilibrium when the VDF is a kappa function instead of a Maxwellian. Therefore (58) generalizes the usual exponential barometric density distribution generally employed in the theory of planetary atmosphere. However, while in the later case (Maxwellian) the temperature is independent of the altitude, in the former case (kappa function), we will see that the temperature increases with the altitude.

Electric Potential Distribution

The expressions giving the densities in an ion exosphere depend on the electrostatic potential $V(\mathbf{r})$. In order to maintain charge neutrality in the plasma, $V(\mathbf{r})$ must be solution of the Poisson's equation:

$$\Delta V = -\sum_j Z_j n_j e/\epsilon_0. \tag{59}$$

This solution is very close to that corresponding to quasi-neutrality [see *Lemaire and Scherer* 1970]:

$$\sum_j Z_j n_j = 0. \tag{60}$$

This is why we solve the algebric non linear equation (58) instead of the second-order differential equation (57) to determine the electrostatic potential $V(\mathbf{r})$ for the range of altitudes considered in Figures 2 to 4.

The solution of the quasi-neutrality condition (58) is straightforward when only electrons and one ion species are forming the ion exosphere. Indeed, in this case, quasi-neutrality $n_e(\mathbf{r}) = n_i(\mathbf{r})$ implies that $q_e(\mathbf{r}) = q_i(\mathbf{r})$ when the densities are given by (58) for both electrons and ions, provided the quasi-neutrality is satisfied at the reference level: $n_{0e} = n_{0i}$. It can be verified from the definition of $q_e(\mathbf{r})$ and $q_i(\mathbf{r})$ given by Eq. (3) that, when $T_{0e} = T_{0i}$, the electrostatic potential distribution maintaining quasi-neutrality of the exospheric plasma corresponds to the Pannekoek-Rosseland (P-R) potential [*Pannekoek*, 1922; *Rosseland*, 1924]. This polarization potential is given by

$$V(\mathbf{r}) = -\frac{m_i - m_e}{2e} \phi_g(\mathbf{r}). \tag{61}$$

The electric field $E = -\nabla V$ is directed upward in the opposite direction to the gravitational field.

When more than one ion species ($O^+, H^+, He^+, \cdots$) and several different populations of electrons (thermal ionospheric electrons, photoelectrons, magnetospheric electrons) constitute the ion-exospheric plasma in barometric equilibrium, the Pannekoek-Rosseland electric field is given by

$$eE = -\frac{\sum_j Z_j m_j n_j / k T_j}{\sum_j Z_j^2 n_j / k T_j} g, \tag{62}$$

provided the pitch angle distributions (PAD) of all charged particle species are isotropic, that is, in barometric equilibrium. Note that this formula is applicable even when the temperature of the electrons and ion species are not the same.

The electric charge density which produces this nonuniform electrostatic potential distribution is extremely small: $(n_{H^+} - n_e)/n_e = 4 \times 10^{-37}$ when no other ions than H^+ ions are present [*Lemaire and Scherer*, 1970]. In the case of a multi-ion exosphere, it can be verified that the space charge density is larger but still negligibly small: $\sum_i Z_i n_i / n_e = 10^{-15}$ in the regions where the densities of the two different ion species (e.g. O^+ and H^+) are comparable.

The P-R electric potential (59) and electric field (60) have been determined above for a Maxwellian VDF with isotropic pitch angle distribution. It is also valid when the VDF of the electrons and ions have the same PAD anisotropy or are truncated in the same range of pitch angles. The P-R potential is also applicable when the VDFs of the charged particles are given by a Lorentzian VDF provided all particles have the same index κ, that is, $\kappa_e = \kappa_i$. Indeed, in this case, the electron and ion densities are everywhere equal to each other, provided $q_e(\mathbf{r}) = q_i(\mathbf{r})$ and $n_{0e} = n_{0i}$. The former equation leads again to the P-R potential (59). Note however that when the VDF is Lorentzian and $\kappa_e \neq \kappa_i$, simple relations between the electric and gravitational potentials and fields like (59) or (60) do not exist. An iterative Newton numerical method must be used to determine $V(\mathbf{r})$ for each altitude as it is done by *Lemaire and Scherer* [1970] and others.

Total Potential Energy Distribution

Figure 2 shows the values of the normalized gravitational (dashed lines), electrostatic (dotted lines) and total potential (solid lines) for protons (top panel) and for electrons (bottom panel) versus altitude, in a barometric model where $T_{0e} = T_{0i}$ and $V(\mathbf{r})$ is given by the P-R formula (59). As indicated above, the quasi-neutrality condition is satisfied by this potential distribution for a Lorentzian VDF provided the electrons VDF and ions VDF have exactly the same index: $\kappa_e = \kappa_i$. Note that the upper solid line giving $q_i(\mathbf{r})$ is exactly the same as the lower solid line giving $q_e(\mathbf{r})$. Both q_i and q_e are increasing functions of $\mathbf{r}$. Therefore the set of formulae corresponding to case (a) must be used to determine the densities, fluxes, pressure tensor components, energy fluxes of the different classes of particles considered in Table 1 (i.e. ballistic, trapped, escaping, incoming).

Figure 3 illustrates the relative abundance of ballistic, trapped, escaping and incoming electrons or protons versus altitude in a protonosphere in barometric equilibrium. The dashed lines correspond to the Maxwellian VDF with densities normalized to the reference level density $n_{0e} = n_{0i} = 300\,\mathrm{cm}^{-3}$. The temperatures of the electrons and H^+ ions are the same: $T_{0e} = T_{0i} = 4000\,\mathrm{K}$. These density distributions are identical to those calculated by *Lemaire* [1976] for a nonrotating ion exosphere. The solid lines correspond to the Lorentzian VDF with the same thermal velocity w and the same density n_0 at the reference level.

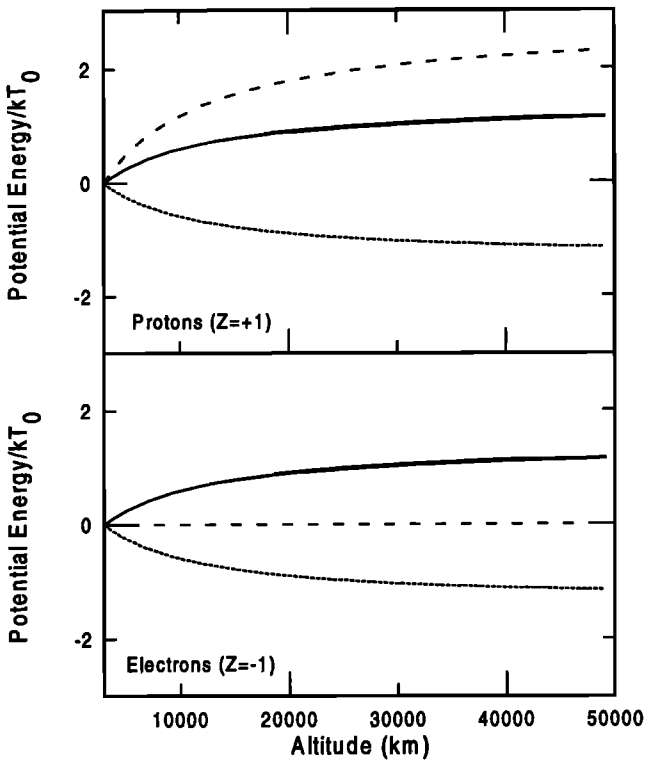

Figure 2. Gravitational (dashed line), electric (dotted line), and total potential energy (solid line) divided by kT_0 as a function of the altitude for (top) protons and (bottom) electrons in the quasi-neutral ion exosphere.

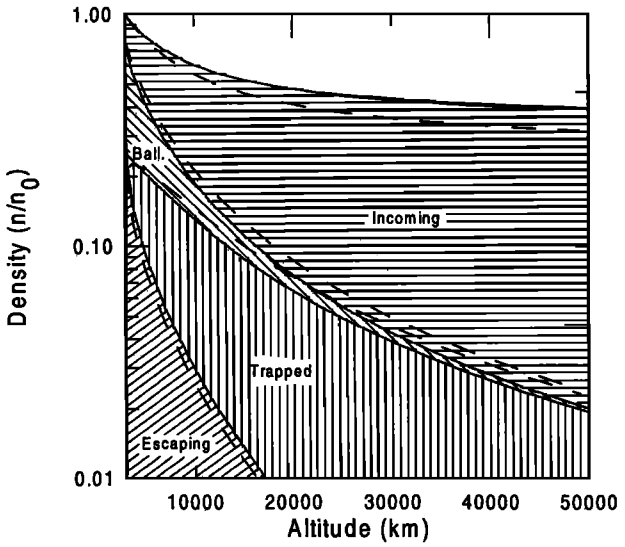

Figure 3. Normalized number density of escaping, trapped, ballistic and incoming electrons as a function of the altitude in the Maxwellian (dashed lines) and in the kappa ($\kappa = 5$, solid lines) models.

The two upper lines represent the total densities given respectively by (55) and (56). It can be seen that when the VDF has an enhanced tail of suprathermal particles approximated by a kappa or Lorentzian function, the total density in the exosphere is larger (upper solid line) than in the classical case of a Maxwellian VDF (upper dashed lines).

Temperature Distribution

We have already shown in Figure 1 how the slope of the Kappa VDF decreases with altitude in an attractive potential distribution. As a consequence, the temperature characterizing the dispersion of velocities increases as a function of altitude.

One can always define parallel and perpendicular kinetic temperatures which are related respectively to the parallel and perpendicular kinetic pressures $P_{\|}$ and $P_{\perp}$ by

$$kT_{\|}(\mathbf{r}) = P_{\|}(\mathbf{r})/n(\mathbf{r}),\ kT_{\perp}(\mathbf{r}) = P_{\perp}(\mathbf{r})/n(\mathbf{r}). \quad (63)$$

When the PAD is isotropic (i.e. $\xi = \zeta = 1$), the parallel and perpendicular temperatures are equal: $T_{\|}(\mathbf{r}) = T_{\perp}(\mathbf{r}) = T(\mathbf{r})$. In this case, there is no temperature anisotropy.

In the Lemaire and Scherer's model with the Maxwellian VDF, the temperature does not depend on the altitude; that is, the temperature distribution is uniform:

$$T(\mathbf{r}) = T_0. \quad (64)$$

This is a consequence of the separability of the spatial (r) and velocity (v) variables in the Maxwellian VDF.

On the other hand, when the VDF is Lorentzian and the PAD isotropic, the density profile is given by (56) and the isotropic pressure becomes simply

$$P(\mathbf{r}) = n_0 k T_0 \frac{\kappa}{\kappa - 3/2}\left(1 + \frac{R(\mathbf{r})}{\kappa w^2}\right)^{-\kappa+3/2} \quad (65)$$

It results from (63) and (56) that the temperature distribution versus altitude is given by

$$T(\mathbf{r}) = \frac{P(\mathbf{r})}{n(\mathbf{r})k} = T_0 \frac{\kappa}{\kappa - 3/2}\left(1 + \frac{R(\mathbf{r})}{\kappa w^2}\right). \quad (66)$$

Since $q(\mathbf{r}) = R(\mathbf{r})/w^2$ increases with the altitude, $T(\mathbf{r})$ will also increase with the altitude.

It can be seen that when $\kappa \to \infty$ (i.e. in the limit of a Maxwellian VDF), (64) becomes identical to (62) and the ion exosphere is isothermal. When $q(\mathbf{r})$ is positive and increasing function of r (i.e. when $dq/dr > 0$), the temperature gradient is also positive: $dT/dr = T_0(dq/dr)/(\kappa - 3/2)$. The smaller κ, the larger the temperature gradient.

The three solid curves in Figure 4 show the increasing temperature $T(\mathbf{r})$ as a function of the altitude for three different values of κ in the barometric model when the PAD is isotropic: $T_{0e} = T_{0i} = 4000\,\mathrm{K}$. When the temperatures T_{0e} and T_{0H+} and the indexes $\kappa_e = \kappa_{H+}$ are identical, the electron and ion temperatures are equal to each other at all altitudes: $T_e(\mathbf{r}) = T_{H+}(\mathbf{r})$.

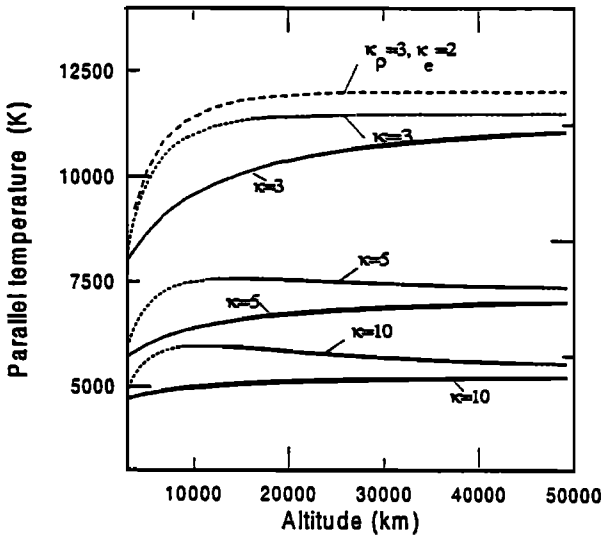

Figure 4. Temperature of electrons and protons as a function of the altitude in the Lorentzian model for different values of κ. The solid curves correspond to barometric models ($\xi = \zeta = 1$) when the pitch angle distribution is isotropic: $T_{\|}(\mathbf{r}) = T_{\perp}(\mathbf{r})$. The dotted lines give the parallel temperature $T_{\|}(\mathbf{r})$ in an ion exosphere when $\kappa_e = \kappa_i$ and when trapped particles are missing in the VDF ($\xi = 0, \zeta = 1$). The dashed line corresponds to the parallel temperature of H^+ ions when $\xi = 0$ and $\zeta = 1$ (i.e. trapped particles missing in PAD) and when the kappa index is smaller for the electrons ($\kappa = 2$) than for H^+ ions ($\kappa = 3$).

The three dashed curves give the distribution of parallel temperatures $T_{\|}(\mathbf{r})$ for three values of the index κ when the trapped particles are missing in the Lorentzian VDF ($\xi = 0$, $\zeta = 1$). The lower dashed curve ($\kappa = 10$, $\xi = 0$) is almost identical to that shown in Figure 5 of *Lemaire* [1976] for a truncated Maxwellian VDF when trapped particles are missing in his nonrotating ion exosphere model.

It can be seen that the dispersion of velocities along magnetic field lines is considerably enhanced in such an anisotropic exospheric model where the PAD is "cigar-like." Cigarlike PAD have been observed during the early refilling phase of a plasmaspheric flux tube which had been emptied during a peeling off event of the plasmasphere [*Sojka and Wrenn*, 1985]. It can be seen that during this early refilling phase when the population of trapped particles is depleted or underpopulated (i.e. when only ballistic, escaping and incoming particles are populating the flux tube), the parallel temperature in the ion exosphere is much larger than at later on when the PAD becomes isotropic due to Coulomb collisions [*Lemaire*, 1989]. The time evolution of the parallel temperature in a refilling flux tube has been simulated numerically by *Lin et al.* [1992, 1994] and *Wilson et al.* [1992, 1993]. Before reaching the Maxwellian equilibrium state in these simulations, positive temperature gradients are also obtained as a result of the upward ionization flow. However, since a Maxwellian VDF is assumed at the reference level in these semikinetic simulations, the temperature profile evolves toward a state of isothermal equilibrium. If a kappa VDF would have been used instead of a Maxwellian, we suspect that their final equilibrium temperature profile would have been similar to those obtained in this paper and shown in Figure 4.

Satellite observations have indicated that the ion temperature increases with altitude along magnetic field lines in the outermost flux tubes of the plasmasphere and plasmathrough where the plasma density is low and the collision frequency small [*Gringauz*, 1985; *Comfort et al.*, 1985]. The collisionless formalism is available in these regions due to their low densities. In the inner plasmasphere, the collisions cannot be neglected. Nevertheless, the collisionless formalism with a kappa can be used to provide zero-order approximations for $n(\mathbf{r})$ and $T(\mathbf{r})$ which we expect to be not drastically different from the more rigorous solutions of the Fokker-Planck equation. Indeed, high-energy particles are much less affected by Coulomb collisions than the core of thermal particles. These exospheric (or zero-order kinetic) solutions are analytic and therefore useful reference models to be compared with the more rigorous but also much more complex solutions of the Fokker-Planck equation.

On the Origin of non-Maxwellian VDF

It has been reemphasized by *Fahr and Shizgal* [1983] and *Shizgal et al.* [1986] that the VDF should be non-Maxwellian in the transition region between the collisionless and collision-dominated region due to the Jeans escape of particles with velocities larger than the critical escape velocity. In partially depleted flux tubes, a VDF with suprathermal tails and significant departures from an isotropic Maxwellian VDF is easier to maintain than deeper inside the plasmasphere and ionosphere where the Coulomb collision frequency is much higher. Therefore it is possible that along field line close to and beyond the plasmapause, increasing temperature gradients are the consequence of the departure of the ion VDF from an isotropic Maxwellian one. Indeed, in a collision dominated plasma, the suprathermal ions have a smaller Coulomb collision cross section than the thermal particles. They tend to develop VDFs with a suprathermal tail. This is also supported by *Livi and Marsch* [1987] for solar wind ion VDF. Suprathermal tails can be simulated by reducing the value of the index κ. Since the "velocity filtration effect" favors the escape of suprathermal ions out of the topside ionosphere, one expects the plasmaspheric temperatures to be higher than those in the underlying ionosphere.

The polar wind proton distributions in the topside transition region have first been modelled by *Barghouthi et al.* [1993]. In their Monte Carlo simulations, these authors have used a Maxwellian VDF at the reference level in the collision-dominated region. They obtained a bean type distribution at high altitude in the collisionless region. It would be interesting to use the same simulation with a VDF having a suprathermal tail (e.g. a kappa function) and compare the new simulation with our analytical results, as well as with their earlier Monte Carlo simulation for a Maxwellian VDF.

Note that alternative theories exist to explain positive temperature gradients in the terrestrial plasmasphere. The most popular is to assume that the upper layers of the plasmasphere are heated by wave-particule interactions whose energy supplied by the ring current and that heat conducted downward [*Olsen*, 1987]. Recently, computer simulations have shown that the electromagnetic proton cyclotron instability driven by the hot magnetospheric proton anisotropy heats cold protons to form anisotropic warm distributions in both the plasmasphere and the outer magnetosphere [*Gary et al., 1995*]. On the other hand, *Kozyra et al.* [1987] use the ring current through Coulomb collisions to heat the near-equatorial plasmasphere. Photoelectrons have also been used to explain some aspects of the measured inner-middle plasmasphere-ionosphere temperature and ion density distributions [*Horwitz et al.*, 1990; *Comfort*, 1996].

Without rejecting these alternative theories, we propose here that if not all, at least part of the observed positive temperature gradient in the topside ionosphere and in the plasmathrough, can be accounted for by the departure of the VDF from the usual Maxwellian VDF, that is, by the relative enrichment of suprathermal ions in the VDF. The enrichment of the population of particles with larger velocity may be explained qualitatively as the consequence of the filtering effect of Coulomb collisions whose cross section is strongly dependent of the relative speed of the colliding charged particles.

Scudder [1992a] argued that the high coronal temperature can be explained by a similar way, without the need of additional heat deposition or dissipation of wave energy in the solar corona. Instead of the 3-D Lorentzian VDF (equation (4) used in this paper), *Scudder* [1992a, b] has considered a 1-D Lorentzian VDF along the vertical direction. Under these circumstances, the density profile is $n(\mathbf{r}) = n(\mathbf{r}_0)(1 + R/\kappa w^2)^{-\kappa-1/2}$ and the pressure $P(\mathbf{r}) = P(\mathbf{r}_0)(1 + R/\kappa w^2)^{-\kappa+1/2}$. Note that for a 3-D Kappa VDF, the exponents of $(1 + R/\kappa w^2)$ in Eqs. (56) and (64) are respectively $-\kappa + 1/2$ and $-\kappa + 3/2$. But the temperature distributions varies as $(1 + R/\kappa w^2)$ in both the 1-D and 3-D case.

Fluxes of Escaping Particles

Since the incoming and escaping fluxes are equal and opposed in barometric models ($\xi = \zeta = 1$), the total flux is then equal to zero for the Maxwellian VDF and the Kappa VDF. But the flux of escaping (and incoming) electrons and H^+ ions are larger in absolute values in the latter model (see Table 3). The larger flux when $\kappa \neq \infty$ is due to the presence of suprathermal particles in the tail of the Lorentzian VDF.

Conclusions

The observed VDFs in the magnetosphere, outer plasmasphere and plasmathrough usually display an enriched population of suprathermal ions which has a power law energy spectrum. It can therefore be simulated by a Lorentzian VDF with an index κ of the order of 3-5, instead of a Maxwellian one which leads to an exponential energy spectrum at suprathermal velocities. This departure of the VDF from a Maxwellian develops most easily in the exobase region where the

Table 3. Escaping Electrons and Hydrogen Ions for a Maxwellian and for Lorentzian VDFs With Different Values of κ and a Pannekoek-Rosseland Electric Potential Distribution

Particle	Flux of Electrons, $cm^{-2}s^{-1}$	Flux of Protons, $cm^{-2}s^{-1}$
Maxwellian	1.75×10^5	4.08×10^3
$\kappa = 100$	1.78×10^5	4.17×10^3
$\kappa = 10$	2.04×10^5	4.77×10^3
$\kappa = 5$	2.38×10^5	5.58×10^3
$\kappa = 3$	2.93×10^5	6.84×10^3

mean free path of particles with an average thermal velocity becomes equal to the local density scale height, that is, in the transition region between the collision dominated ionosphere and the collisionless ionosphere.

We have established the expression of the density distribution in an ion exosphere in the case when the velocity distribution function is a Lorentzian function instead of a 3-D Maxwellian one. We have generalized the ion exosphere models developed by *Lemaire and Scherer* [1970, 1971, 1973] for truncated Maxwellian VDFs which correspond to the special case $\kappa = \infty$.

We have calculated separately the contributions of the different categories of escaping, ballistic, trapped and incoming ions and electrons to the total barometric density, flux, parallel and perpendicular pressures and energy flux. The density gradient along magnetic field lines in a barometric model decreases when the index κ is reduced from its limiting value $\kappa = \infty$ to $\kappa = 3 - 5$ which fit approximately the observed VDF in the magnetospheric plasmas. When the VDF is a Kappa function, the equatorial plasmaspheric density is enhanced with respect to the Maxwellian case. This means that the field-aligned density distribution in a saturated flux tube is higher for a Lorentzian barometric model than in the case of the Maxwellian barometric model.

Furthermore we have determined the temperature distribution in a barometric Lorentzian ion exosphere formed by H^+ ions and electrons of the same temperature at a reference level of 3000 km altitude. We have shown that the temperature increases with altitude along the field lines from 8000 K at 3000 km to more than 12000 K at 40000 km when $\kappa = \kappa_e = \kappa_i$ is reduced to a value of 3. Larger field-aligned temperature gradients can be obtained when the index κ is smaller than 3.

One obtains higher parallel temperatures when the trapped particles are removed. The positive temperature gradients are a consequence of the non Maxwellian character of the VDF. It is not produced by additional energy dissipation due to some wave-particle interaction mechanism. When the value of κ_e is smaller than κ_i, an additional temperature is obtained both for the H^+ ions and electrons.

Acknowledgments. The authors wish to thank the Director of IASB and the Science Policy Office for their support. J. D. Scudder is acknowledged for some enlightenments concerning the "velocity filtration effect". His pioneer work has inspired the present application of the velocity filtration mechanism to the terrestrial plasmasphere.

The Editor thanks Bernie Shizgal and James L. Horwitz for their assistance in evaluating this paper.

References

Bame, S. J., J. R. Asbridge, H. E. Felthauser, E.W. Hones Jr., and I. B. Strong, Characteristics of the plasma sheet in the Earth's magnetotail, *J. Geophys. Res., 72,* 113, 1967.

Barghouthi, I. A., A. R. Barakat, and R. W. Schunk, Monte Carlo study of the transition region in the polar wind: An improved collision model, *J. Geophys. Res., 98,* 17583, 1993.

Chiu, Y. T., and M. Schulz, Self-consistent particle and parallel electrostatic field distributions in the magnetospheric-ionospheric auroral region, *J. Geophys. Res., 83,* 629, 1978.

Chiu, Y. T., A. L. Newman, and J. M. Cornwall, On the structures and mapping of auroral electrostatic potentials, *J. Geophys. Res., 86,* 10029, 1981.

Christon, S. P., D. G. Mitchell, D. J. Williams L. A. Frank, C. Y. Huang, and T. E. Eastman, Energy spectra of plasma sheet ions and electrons from $\sim$ 50 eV/e to $\sim$ 1 MeV during plasma temperature transitions, *J. Geophys. Res., 93,* 2562, 1988.

Comfort, R. H., Thermal structure of the plasmasphere, *Adv. Space Res., 10*(10), 175, 1996.

Comfort R. H., J. H. Waite, and C. R. Chappell, Thermal ion temperatures from the retarding ion mass spectrometer on DE 1, *J. Geophys. Res., 90,* 3475, 1985.

Fahr, H. J., and B. Shizgal, Modern exospheric theories and their observational relevance, *Rev. Geophys., 21,* 75, 1983.

Fälthammar, C.-G., Magnetic-field-aligned electric fields, *Eur. Space Agency J., 7,* 385, 1983.

Farrugia, C. J., D. T. Young, J. Geiss, and H. Balsiger, The composition, temperature and density structure of cold ions in the quiet terrestrial plasmasphere: GEOS 1 results, *J. Geophys. Res., 94,* 11865, 1989.

Fridman, M., and J. Lemaire, Relationship between auroral electrons fluxes and field-aligned electric potential difference, *J. Geophys. Res., 85,* 664, 1980.

Gary, S. P., M. F. Thomsen, L. Yin, and D. Winske, Electromagnetic proton cyclotron instability: Interactions with magnetospheric protons, *J. Geophys. Res., 100,* 21,961, 1995.

Gloeckler, G., and D. C. Hamilton, AMPTE ion composition results, *Phys. Scr., T18,* 73, 1987.

Gringauz, K. I., Structures and properties of the Earth's plasmasphere, *Adv. Space Res., 5*(4), 391, 1985.

Gringauz, K. I., and V. V. Bezrukikh, Asymmetry of the Earth's plasmasphere in the direction noon-midnight from PROGNOZ and PROGNOZ-2 data, *J. Atmos. Terr. Phys., 38,* 1071, 1976.

Hinton, F. L., Collisional transport in plasma, in *Handbook of Plasma Physics,* Edited by M. N. Rosenbluth and R. Z. Sagdeev, pp. 147, North-Holland Publishing Company, Amsterdam, 1983.

Horwitz, J. L., R. H. Comfort, P. G. Richards, M. O. Chandler, C. R. Chappell, P. Anderson, W. B. Hanson, and L. H. Brace, Plasmasphere-ionosphere coupling, II, Ion composition measurements at plasmaspheric and ionospheric altitudes and comparison with modeling results, *J. Geophys. Res., 95,* 7949, 1990.

Knight, L., Parallel electric fields, *Planet. Space Sci., 21,* 741, 1973.

Kozyra, J. U., E. G. Shelley, R. H. Comfort, L. H. Brace, T. E. Cravens, and A. F. Nagy, The role of ring current O^+ in the formation of stable auroral red arcs, *J. Geophys. Res., 92,* 7487, 1987.

Lemaire, J., Rotating ion exospheres, *Planet. Space Sci., 24,* 975, 1976.

Lemaire, J., Plasma distribution models in a rotating mag-

netic dipole and refilling of plasmaspheric flux tubes, *Phys. Fluids B, 1*, 1519, 1989.

Lemaire, J., and M. Scherer, Model of the polar ion exosphere, *Planet. Space Sci., 18*, 103, 1970.

Lemaire, J., and M. Scherer, Simple model for an ion exosphere in an open magnetic field, *Phys. Fluids, 14*,(8), 1683, 1971.

Lemaire, J., and M. Scherer, Plasma sheet particle precipitation: A kinetic model, *Planet. Space Sci., 21*, 281, 1973.

Lemaire, J., and M. Scherer, Exospheric models of the topside ionosphere, *Space Sc. Rev., 15*, 591, 1974.

Lemaire, J., and M. Scherer, Field-aligned current density versus electric potential characteristics for magnetospheric flux tubes, *Ann. Geophys., 1*, 91, 1983.

Lin, J., J. L. Horwitz, G. R. Wilson, C. W. Ho, and D. G. Brown, A semikinetic model for early stage plasmaspheric refilling, II, Effects of wave-particle interactions, *J. Geophys. Res., 97*, 1121, 1992.

Lin, J., J. L. Horwitz, G. R. Wilson, and D. G. Brown, Equatorial heating and hemispheric decoupling effects on inner magnetospheric core plasma evolution, *J. Geophys. Res., 99*, 5727, 1994.

Livi, S., and E. Marsch, Generation of solar wind proton tails and double beams by Coulomb collisions, *J. Geophys. Res., 92*, 7255, 1987.

Lui, T. Y., and S. M. Krimigis, Earthward transport of energetic protons in the Earth's plasma sheet, *Geophys. Res. Lett. , 8*, 527, 1981.

Lui, T. Y., and S. M. Krimigis, Energetic ion beam in the Earth's magnetotail lobe, *Geophys. Res. Let. , 10*, 13, 1983.

Lyons, L. R., Generation of large-scale regions of auroral currents, electric potentials, and precipitation by the divergence of the convection electric field, *J. Geophys. Res., 85*, 17, 1980.

Lyons, L. R., Discrete aurora as a direct result of an inferred high-altitude generating potential distribution, *J. Geophys. Res., 86*, 1, 1981.

Miyamoto K., *Plasma Physics for Nuclear Fusion*, MIT Press, Cambridge, Mass., 1987.

Norris, A. J., J. J. Sojka, G. L. Wrenn, J. F. Johnson, N. Cornilleau, S. Perraut, and A. Roux, Experimental evidence for the acceleration of thermal electrons by ion cyclotron waves in the magnetosphere, *J. Geophys. Res., 88*, 889, 1983.

Olsen, R. C., S. D. Shawhan, D. L. Gallagher, J. L. Green, C. R. Chappell, and R. R. Anderson, Plasma observations at the Earth's magnetic equator, *J. Geophys. Res., 92*, 2385, 1987.

Pannekoek, A., Ionization in stellar atmospheres, *Bull. Astron. Inst. Neth., 1*, 107, 1922.

Rosseland, S., Electric state of a star, *Mon. Not. R. Astron. Soc., 84*, 720, 1924.

Scudder, J. D., On the causes of temperature change in inhomogeneous low-density astrophysical plasmas, *Astrophys. J., 398*, 299, 1992a.

Scudder, J. D., Why all stars possess circumstellar temperature inversions, *Astrophys. J. , 398*, 319, 1992b.

Shizgal, B., U. Weinert, and J. Lemaire, Collisional kinetic theory of the escape of light ions from the polar wind, *Rarefied Gas Dyn., 2*, 374, 1986.

Sojka, J. J., and G. L. Wrenn, Refilling of geosynchronous flux tubes as observed at the equator by GEOS 2, *J. Geophys. Res., 90*, 6379, 1985.

Spitzer, L., Jr., *The Atmospheres of the Earth and Planets*, edited by G. P. Kuiper, pp. 213–249, Univ. Chicago Press, Chicago, Ill., 1949.

Spitzer, L., Jr., *Physics of Fully Ionized Gases*, 105 pp., Interscience, New York, 1956.

Stern, D. P., One-dimensional models of quasi-neutral parallel electric fields, *J. Geophys. Res., 86*, 5839, 1981.

Williams, D. J., D. G. Mitchell, and S. P. Christon, Implications of large flow velocity signatures in nearly isoand tropic ion distributions, *Geophys. Res. Lett., 15*, 303, 1988.

Wilson, G. R., J. L. Horwitz, and J. Lin, A semikinetic model for early stage plasmaspheric refilling: Effects of Coulomb collisions, *J. Geophys. Res., 97*, 1109, 1992.

Wilson, G. R., J. L. Horwitz, and J. Lin, Semikinetic modeling of plasma flow on outer plasmaspheric field lines, *Adv. Space Res., 13*(4), 107, 1993.

V. Pierrard and J. Lemaire, Institut d'Aéronomie Spatiale de Belgique, B-1180, Brussels, Belgium.

(Received March 27, 1995; revised November 23, 1995; accepted December 7, 1995.)